Application of cryptocrystalline magnesite-bentonite clay hybrid for defluoridation of underground water resources: implication for point of use treatment

V. Masindi

ABSTRACT

A new synthesis method was established to fabricate a nanocomposite material comprising of cryptocrystalline magnesite and bentonite clay that has high adsorption capacity for ionic pollutants. To synthesize the composite at 1:1 weight (g): weight (g) ratio, a vibratory ball mill was used. Batch adsorption experiments were carried out to determine optimum conditions for fluoride adsorption. Parameters optimized included: time, dosage, concentration and pH. Optimum conditions for defluoridation were found to be 30 min of agitation, 0.5 g of dosage, 0.5:100 solid to liquid (S/L) ratios and 25 mg L^{-1} of initial fluoride ions. Fluoride removal was independent of pH. The adsorption kinetics and isotherms were well fitted by pseudo-second-order and Langmuir models, respectively, indicating chemical and monolayer adsorption. Findings illustrated that the newly synthesized adsorbent was a promising adsorbent for the environmental pollution clean-up of excess fluoride in underground water and it can be used as a point source treatment technology in rural areas of South Africa and other developing countries.

Key words | adsorption, bentonite clay, cryptocrystalline magnesite, defluoridation, fluoride, magnesite-bentonite composite

V. Masindi
CSIR (Council of Scientific and Industrial Research), Built Environment, Hydraulic and Infrastructure Engineering,
P.O. Box 395, Pretoria, 0001,
South Africa
and
Department of Environmental Sciences, School of Agriculture and Environmental Sciences,
University of South Africa (UNISA),
P.O. Box 392, Florida, 1710,
South Africa
E-mail: *VMasindi@csir.co.za*

INTRODUCTION

Fluorosis has become a chronic peril endangering the health of the majority of the population worldwide, especially those living in rural areas (Ayoob & Gupta 2006; Mohapatra *et al.* 2009; Bhatnagar *et al.* 2011; Gitari *et al.* 2013; Zulfiqar *et al.* 2014). In a number of African countries, including Kenya, Tanzania and South Africa, very high levels of fluoride in groundwater (as high as 30 mg L^{-1}) have been reported. Excessive fluoride in drinking water causes the development of dental and skeletal fluorosis in affected populations who source drinking water from untreated groundwater (Gitari *et al.* 2013; Masindi *et al.* 2014c).

Considering the dangers that come with consuming high fluoride waters, a maximum permissible limit of 1.5 mg L^{-1} has been recommended for consumption in potable water (Ayoob & Gupta 2006; Mohapatra *et al.* 2009; Bhatnagar *et al.* 2011; Miretzky & Cirelli 2011; Jagtap *et al.* 2012; Gitari *et al.* 2013; Masindi *et al.* 2014c; Zulfiqar *et al.* 2014). Compared to underground water, surface waters do not always contain fluoride beyond this level. Due to the presence of fluoride-rich minerals as well as hydrogeological conditions of the place the water is sourced, underground water contains this excess fluoride (Gitari *et al.* 2013; Masindi *et al.* 2014c). With fluorosis being a serious health issue, it follows that defluoridation of drinking water has to be practised on those waters that have excessive fluoride levels beyond the recommended limit (Gitari *et al.* 2013; Masindi *et al.* 2014c).

Methods practised for removal of excess fluoride include adsorption (Zhou *et al.* 2004; Tor 2006; Zhu *et al.* 2009; Thakre *et al.* 2010a; Viswanathan & Meenakshi 2010;

doi: 10.2166/wrd.2016.055

Zulfiqar *et al.* 2014; Yu *et al.* 2015), precipitation (Turner *et al.* 2005; Onyango & Matsuda 2006; Zhang *et al.* 2014), coagulation (Khatibikamal *et al.* 2010; Emamjomeh *et al.* 2011; Vasudevan *et al.* 2011; Gong *et al.* 2012; Sandoval *et al.* 2014), filtration (Kettunen & Keskitalo 2000; Mohapatra *et al.* 2009; Maliyekkal *et al.* 2010; Wang *et al.* 2010; Dolar *et al.* 2011), reverse osmosis (Mohapatra *et al.* 2009; Shen & Schäfer 2014; Trikha & Sharma 2014), ion exchange (Ruixia *et al.* 2002; Luo & Inoue 2004; Meenakshi & Viswanathan 2007; Mohapatra *et al.* 2009) and distillation (Hou *et al.* 2010). Limitations of these methods include the daily addition of chemicals; large volumes of sludge production; and some of these methods have been reported as being ineffective with water sources having high total dissolved solids (TDS) (Ayoob & Gupta 2006; Onyango & Matsuda 2006; Mohapatra *et al.* 2009; Bhatnagar *et al.* 2011; Miretzky & Cirelli 2011; Zulfiqar *et al.* 2014).

However, adsorption is one of the techniques, which is comparatively more useful and economical at low pollutant concentration (Onyango & Matsuda 2006; Zulfiqar *et al.* 2014). To that end, it is the defluoridation method that is now widely used in rural areas (Masindi *et al.* 2014c). Many types of low-cost and effective materials have been used as adsorbents in defluoridation which include different clays, tree bark, charcoal, saw dust, alum sludge and red tea waste (Srimurali *et al.* 1998; Çengeloğlu *et al.* 2002; Mohapatra *et al.* 2009; Bhatnagar *et al.* 2011; Jagtap *et al.* 2012; Gitari *et al.* 2013; Masindi *et al.* 2014c; Zulfiqar *et al.* 2014).

Due to their versatility, high surface area, swelling capabilities, cation exchange capacity and abundance, clays and clay minerals have received paramount attention in depollution science (Bhattacharyya & Gupta 2008; Masindi *et al.* 2015a). However, their inorganic species retention capabilities are dependent on pH and species concentrations (Masindi *et al.* 2015a). To respond to those limitations and to minimize the use of virgin materials, clays can be blended with metal oxides and carbonates to improve their adsorption ability for inorganic contaminants (Gitari *et al.* 2013; Masindi *et al.* 2014c, 2015a; Masindi & Gitari 2016). The aim of the present study was to develop a cryptocrystalline magnesite-bentonite clay nanocomposite as a novel technology and evaluate the feasibility of using the fabricated composite for the defluoridation of surface and underground water for use in households.

MATERIALS AND METHODS

Sampling

Fluoride-rich water collected from a community borehole in Siloam village Limpopo Province, South Africa was used to evaluate the effectiveness of the prepared composite adsorbent in the treatment of field water. Raw magnesite rocks from the Folovhodwe Magnesite Mine in Limpopo Province, South Africa, were collected without any prior processing. Bentonite clay was supplied by ECCA Holdings (Pty) Ltd Cape Bentonite mine (Cape Town, South Africa).

Adsorbent preparation

To prepare the material for adsorption processes, the magnesite rock samples were milled into a powder using a Retsch RS 200 mill and afterwards passed through a sieve to obtain 32 μm particle sizes. The raw bentonite was washed by soaking in ultra-pure water for 10 min and thereafter draining the wash. The level of the ultrapure water used was such that it covered the entire sample in the beaker and was allowed to overflow. The procedure was repeated four times. The washed bentonite was dried in an oven (24 h at 105 °C). The dried samples were milled into a fine powder (Retsch RS 200 mill) and sieved (32 μm particle size sieves).

Synthesis of mechanochemical activated composite

The composite adsorbent was synthesized via a mechanochemical method using the following procedure. A vibratory ball mill was used for making the magnesite-bentonite clay composite. Powdered bentonite (500 g) and magnesite (500 g) were mixed on a 1:1 wt% mass ratio. The mixture was crushed and homogenized by pulverizing into a fine powder (Retsch RS 200 mill) for 30 min at 800 rpm. After sieving <32 μm sized particles were obtained and the prepared material was kept in sealed zip-lock plastic bags. The conditions for milling were previously determined as optimal milling parameters for mechanochemical modification of bentonite clay-cryptocrystalline magnesite composite by Masindi (Masindi *et al.* 2014a, 2015a; Masindi & Gitari 2016).

Preparation of working solution

For all the experiments, the accuracy of the analysis was monitored by analysis of National Institute of Standards and Technology (NIST) water standards. Simulated fluoride-rich water was synthesized using sodium fluoride salt. A standard stock solution of fluoride (1,000 mg L^{-1} F) was prepared by dissolving 0.221 g sodium fluoride into 100 mL deionized water from a Milli-Q water system. Fluoride-bearing solutions were prepared by diluting the stock solution to desired concentrations with ultra-pure water.

Determination of fluoride concentration

Fluoride concentrations were measured by a fluoride ion selective electrode (Thermo Scientific Orion Star A215 pH/Conductivity Benchtop Meter (USA) coupled to an 8157BNUMD Orion ROSS Ultra Triode pH/ATC electrode). Before fluoride determination, a total ionic strength adjusting buffer (TISAB III) was added to the solutions in a ratio of 10:1 in order to maintain ionic strength and pH, and eliminate the interference effect of F-ion complexing with metal cations.

Microstructural characterisation

Mineralogical composition of the composite and resulting solid residues was determined using X-ray diffraction (XRD). They were analysed using a PANalytical X'Pert Pro powder diffractometer in θ–θ configuration with an X'Celerator detector and variable divergence, and fixed receiving slits with Fe filtered Co-Kα radiation ($\lambda = 1.789$ Å). The phases were identified using X'Pert Highscore plus software at University of Pretoria, South Africa. Morphology was determined using scanning electron microscopy-electron dispersion spectrometry (SEM-EDS) (JOEL JSM – 840, Hitachi, Tokyo, Japan).

Optimization of adsorption conditions

Optimization experiments were done in batch experimental procedures. Parameters optimized include time, dosage, concentration and pH. All experiments were done in triplicate. Samples of 100 mL of 50 mg L^{-1} F^- solution were pipetted into nine, 250 mL high-density polyethylene plastic bottles and 1 g of the composite added. The mixtures were agitated for varying contact times. The mixtures were then filtered through a 0.45 μm pore nitrate cellulose filter membrane. pH, electrical conductivity (EC) and TDS were measured using a CRISOM MM40 multimeter probe. The samples were refrigerated at 4 °C until analysis by fluoride meter.

Eight, 100 mL solutions of 50 mg L^{-1} F^- were pipetted into eight, 250 mL bottles and varying masses of the composite added. The mixtures were agitated for an optimum time of 30 min at 250 rpm using the Stuart reciprocating shaker. The filtered samples were treated as discussed previously.

Six, 100 mL solutions were pipetted into six, 250 mL bottles with 0.5 g of the composite and 100 mL of the stock solution with different concentrations of fluoride were added into each container. The mixtures were agitated for an optimum time of 30 min at 250 rpm using the Stuart reciprocating shaker. The filtered samples were treated as discussed previously.

Six, 100 mL solutions of 25 mg L^{-1} F^- were pipetted into eight, 250 mL bottles with 0.5 g of the composite and the pH was adjusted from 2 to 12 using NaOH and nitric acid. The mixtures were agitated for an optimum time of 30 min at 250 rpm using the Stuart reciprocating shaker. The filtered samples were treated as discussed previously. The synthetic and fluoride-rich underground water were treated under optimized conditions.

Calculation of the extent of fluoride removal and adsorption capacity

The percentage removals of fluoride by the composite were computed by the expression:

$$\%\ \text{Removal} = \left(\frac{C_i - C_e}{C_i}\right) \times 100 \quad (1)$$

where C_i = initial concentration and C_e = equilibrium ion concentration, respectively.

The amounts of fluoride adsorbed by the composite were determined by the expression:

$$q = \frac{(C_i - C_e)V}{m} \quad (2)$$

where C_i = initial ions concentration (mg L^{-1}), C_e = ions

concentration at equilibrium (mg L^{-1}), V = volume of ions solution (L) and m = weight of the composite in grams.

RESULTS AND DISCUSSION

Microstructural characterizations

X-ray diffraction analysis

The mineralogical composition of magnesite, bentonite clay and magnesite-bentonite clay composite are shown in Figure 1.

XRD analysis showed that magnesite consists of periclase, brucite and forsterite as the main mineral phase. The low intensity peaks indicate that the material is enriched with amorphous phases. Bentonite clay was observed to contain smectite, quartz, plagioclase, calcite and muscovite. Common between the magnesite and bentonite clay is the quartz which also tends to form the highest peaks. XRD pattern of the product synthesized shows one intense diffraction peak around about $2\theta = 27.2^{\circ}$ which is due to quartz. The composite was determined to contain smectite, periclase, quartz, gibbsite and muscovite which are the main components of magnesite and bentonite clay. The presence of gibbsite and quartz substantiates that the material is still an alumino-silicate. Broad peaks indicate that the synthesized composite has amorphous phases thus proving that ball milling can result in amorphization of the material (Kumrić *et al.* 2013; Dukić *et al.* 2015a, 2015b).

Scanning electron microscopy-electron dispersion spectrometry

SEM images of bentonite clay (A), magnesite (B), magnesite-bentonite clay composite (C) and fluoride-reacted composite (D) are shown in Figure 2(a)–2(d).

Figure 2 shows the SEM images of the prepared adsorbents. As shown in Figure 2(a) bentonite clay is characterized by leaf- and plate-like sheets arranged in layered formation. On the contrary, Figure 2(b) shows that magnesite is characterized by rod-like, spherical and sheet-like structures showing its heterogeneous nature. The magnesite-bentonite clay composite was observed to be dominated by spherical particles, honeycomb-like tetrahedral folding of materials meshed together. The leaf- and sheet-like structure were also observed, meaning that the mechanical structure of the clay remained compact (Figure 2(c)). The heterogeneous surface indicates the genesis of the composite to be layered, sheet and rod-like, and spherical structures. The reduction in sheet sizes proves that the material has been fragmented, distorted, and exfoliated. This correlates with results obtained by Dukić *et al.* (2015a). After contacting the fluoride-rich water, the mechanochemical synthesized composite showed the presence of sheets and leaf-like structures thus showing that the mechanical stability of the clay is preserved (Figure 2(d)). The rod-like structures and materials suspended on the reacted composite structures indicate the deposition of materials on the composite surfaces.

Transmission electron microscopy-electron dispersion spectrometry

Transmission electron microscopy (TEM) images and spectra of magnesite, bentonite clay, magnesite-bentonite clay composite and fluoride reacted composite are shown in Figure 3(a)–3(d).

Figure 3(a) displays a cloudy background with sheet-like structures on the cryptocrystalline magnesite. This shows that the material contains amorphous and crystalline phases. The EDS revealed that Mg, C and O are the major components verifying that the material under study is magnesium carbonate. Traces of Ca and Fe were also observed to be present. Such metals also aid in removal of fluoride from wastewaters. The availability of Cu is due to the use of a copper grid.

Figure 3(b) reveals the presence of rod and sheet identical structures. EDS revealed that Al, O and Si are the predominant species. This is indicative of the material being an alumino-silicate. Fe and Mg were also observed to be present hence proving that these are the exchangeable cations which can also aid in the removal of fluoride from underground water.

Figure 3(c) shows the availability of tube- and rod-like structures with a background which is cloudy. This indicates that the material is a blend of magnesite and bentonite clay. Moreover, this shows that the fabricated material contains crystalline and amorphous phases. The EDS disclosed that there is a notable amount of C, O, Si, Mg, and Al thus proving that the material is a blend of magnesite and bentonite clay.

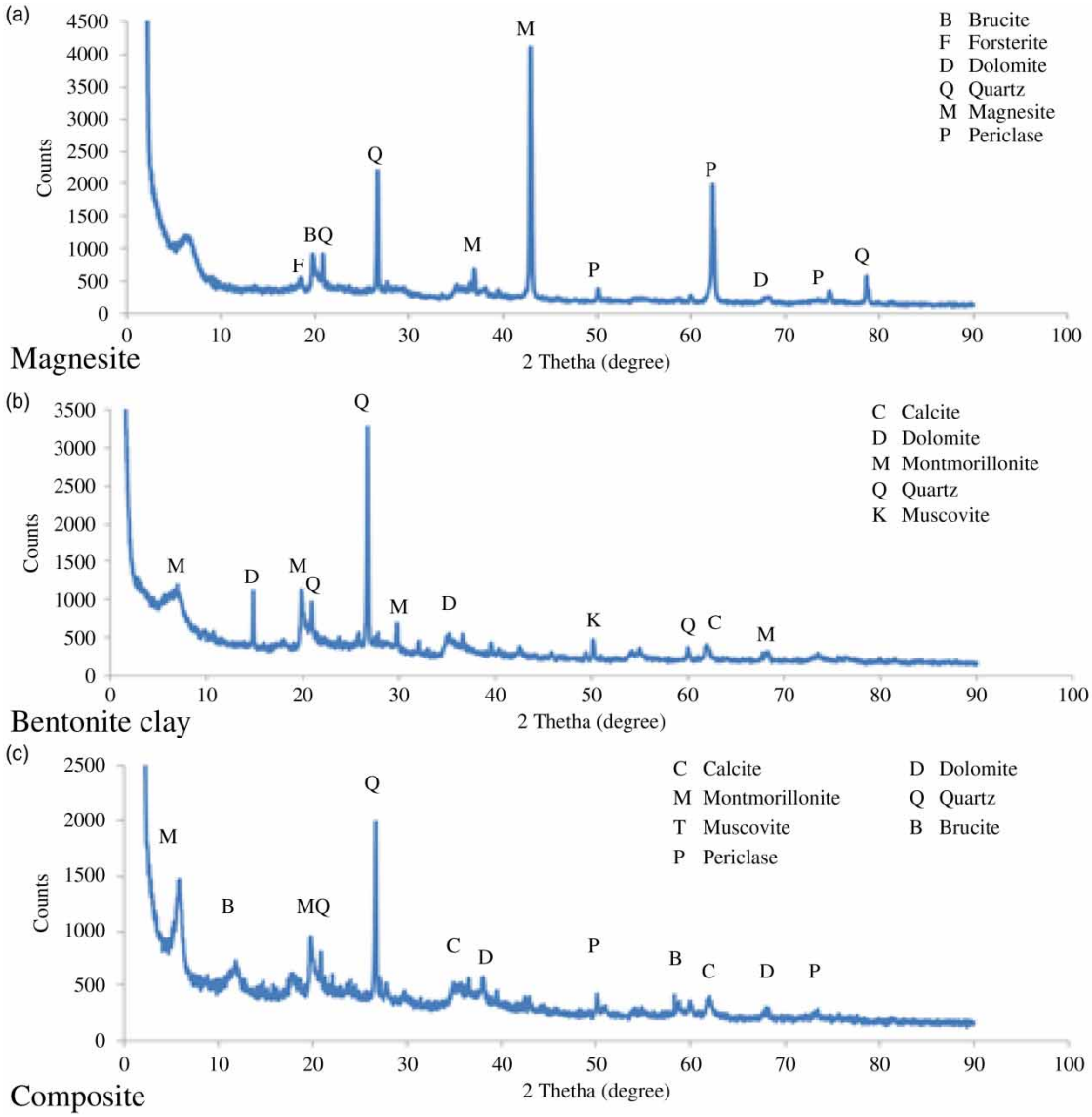

Figure 1 | XRD spectra of magnesite (a), bentonite clay (b) and magnesite-bentonite clay composite (c).

Figure 3(d), like Figure 3(c), shows the availability of tube- and rod-like structures with a cloudy background. EDS proved the addition of fluoride on the composite matrices hence proving that the composite is a sink of fluoride from aqueous solution.

Optimization experiments

Batch experiments were carried out to evaluate the effects of shaking time, dosage, fluoride concentration and pH on removal of fluoride from aqueous solution.

Effect of shaking time

The effect of shaking time on the removal of fluoride from aqueous solution is shown in Figure 4.

As shown in Figure 4, there was a rapid increase in percentage removal of fluoride with an increase in contact time from the first minute of contact time to about 30 min. From 1 to 30 mins, the composite managed to remove >99% of fluoride from the aqueous solution. Thereafter, no significant uptake of fluoride was observed indicating that the reaction kinetics had reached an equilibrium

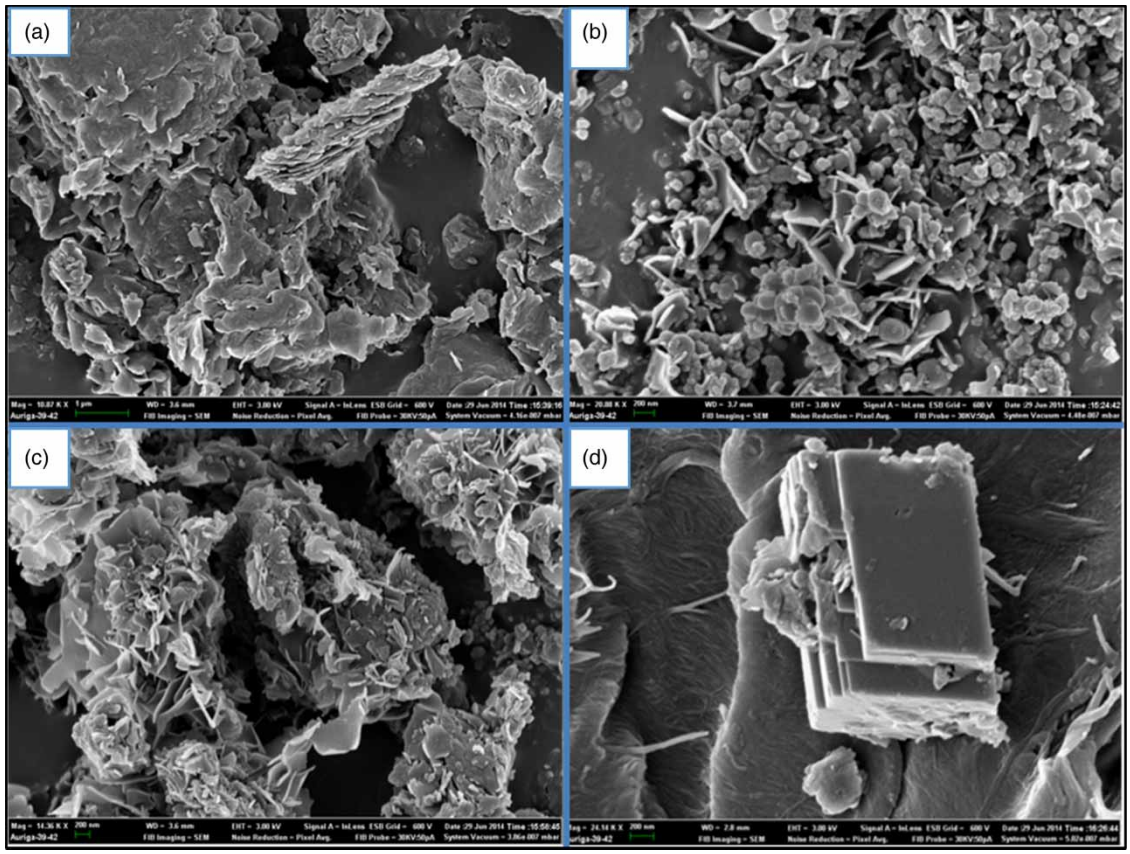

Figure 2 | SEM images of bentonite clay (a), magnesite (b), magnesite-bentonite clay composite (c) and fluoride-reacted composite (d).

state. A possible explanation of this trend is that that the composite provided more surfaces sufficient to remove all the fluorides that were in aqueous solution in the first 30 min. This study showed shorter contact time for removal of fluoride as compared to a study by Thakre *et al.* (2010b) that required 12 h of equilibration for removal of fluoride using magnesium modified bentonite clay. On this basis 30 min was selected as the optimum equilibration time for further optimization experiments.

Effects of dosage

The effect of dosage on the removal of fluoride from aqueous solution is shown in Figure 5.

As shown in Figure 5, the percentage removal of fluoride was observed to increase with an increase in dosage. The percentage removal of fluoride increased rapidly, as the dosage was increased from 0.1 to 0.5 g. The composite managed to remove >99% of fluoride from the aqueous solution. After which, no significant increase in adsorption was observed. High percentage removal is attributed to more surface suitable for adsorption becoming available as the dosage increases. As such, it was concluded that 0.5 g is the optimum dosage for adsorption of 10 mg L^{-1} of fluoride from aqueous solution and it will be used for the following experiments.

Effect of initial fluoride concentration

The effect of initial fluoride concentration on the removal of fluoride from aqueous solution is shown in Figure 6.

The uptake of fluoride by the composite was studied by varying the initial concentration of fluoride from 2 to 50 mg L^{-1}. As shown in Figure 6, there was a high percentage removal of fluoride at low concentrations but as the concentration of fluoride increased the percentage removal

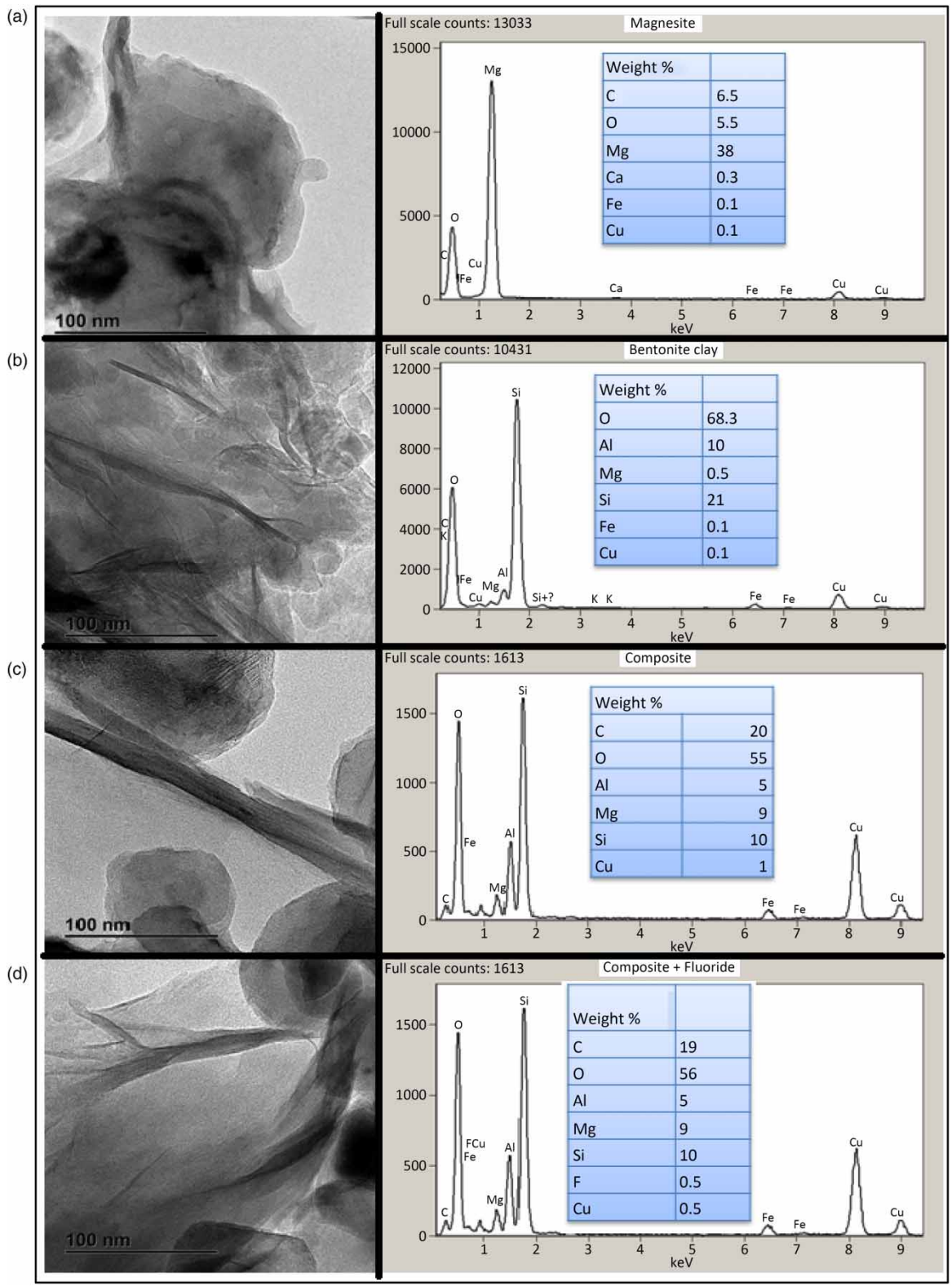

Figure 3 | TEM images and spectra of magnesite (a), bentonite clay (b), magnesite-bentonite clay composite (c) and fluoride-reacted composite (d).

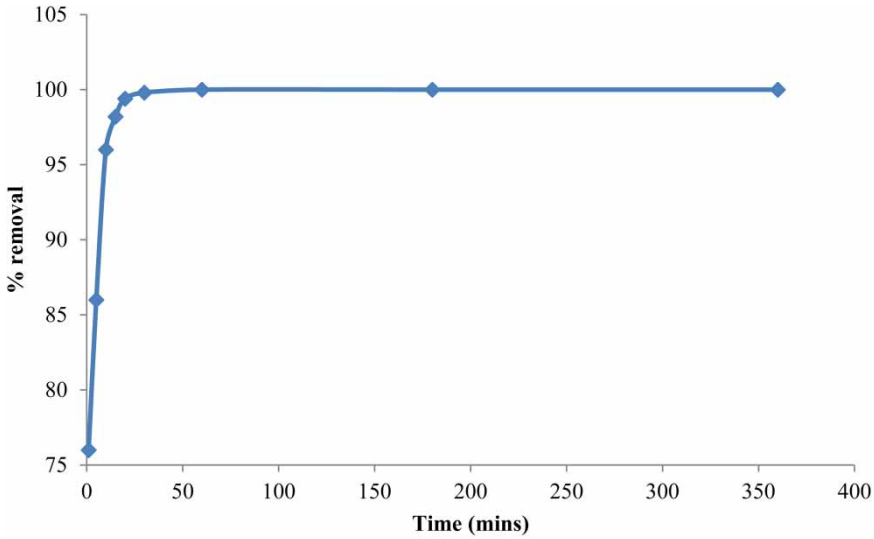

Figure 4 | Percentage removal of fluoride with shaking time (conditions: 1 g dosage, 10 mg L^{-1} of fluoride, pH 10, 250 rpm, 100 mL, 1:100 solid to liquid (S/L) ratio and 26 °C room temperature).

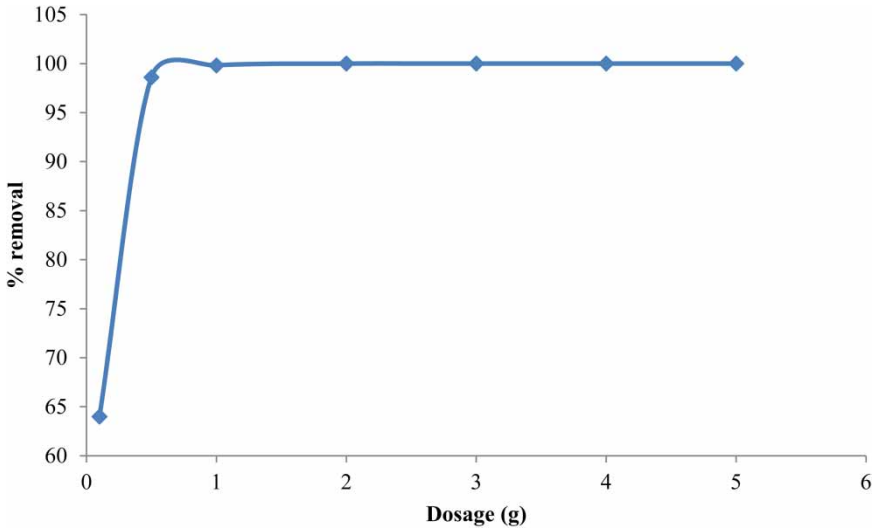

Figure 5 | Percentage removal of fluoride with dosage (conditions: 30 min of shaking, 10 mg L^{-1} of fluoride, pH 10, 250 rpm, 100 mL and 26 °C room temperature).

decreased. High percentage removal at low concentration is attributed to more adsorption sites being available at initial stages, but when the concentration increases more fluoride ion species become available to occupy the vacant surfaces on the composite. However, it was observed that the composite removed >99% of fluoride in the range of 2–25 mg L^{-1}. Based on the observed results, 25 mg L^{-1} of fluoride concentration was taken as the optimum concentration for subsequent experiments.

Effect of supernatant pH

The effect of pH on the removal of fluoride from aqueous solution is shown in Figure 7.

The effect of pH on removal of fluoride from aqueous solution was evaluated from pH 2 to 12. Removal of fluoride by the composite at varying pH was observed to be high over a wide range of pH values (Figure 7). From pH 2 to 12, the removal efficiency was greater than 99%. High adsorption of

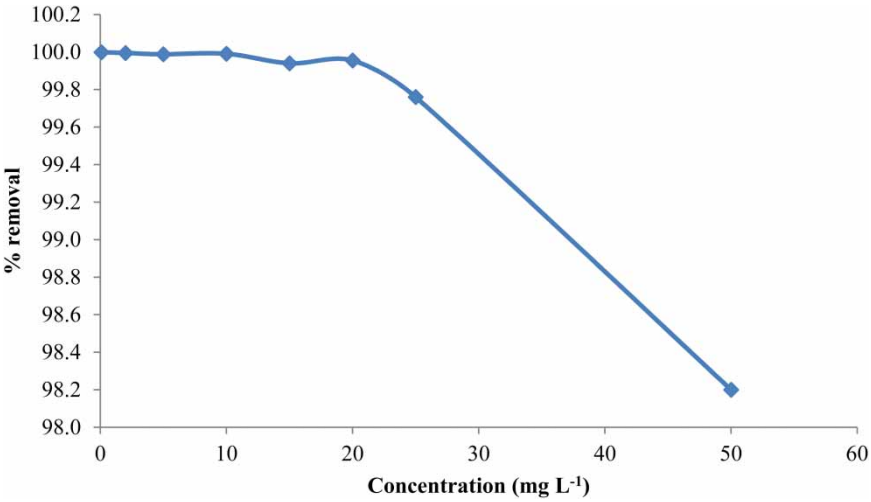

Figure 6 | Percentage removal of fluoride with concentration (conditions: 30 min, 0.5 g, 100 mL, pH 10, 250 rpm, and 26 °C room temperature).

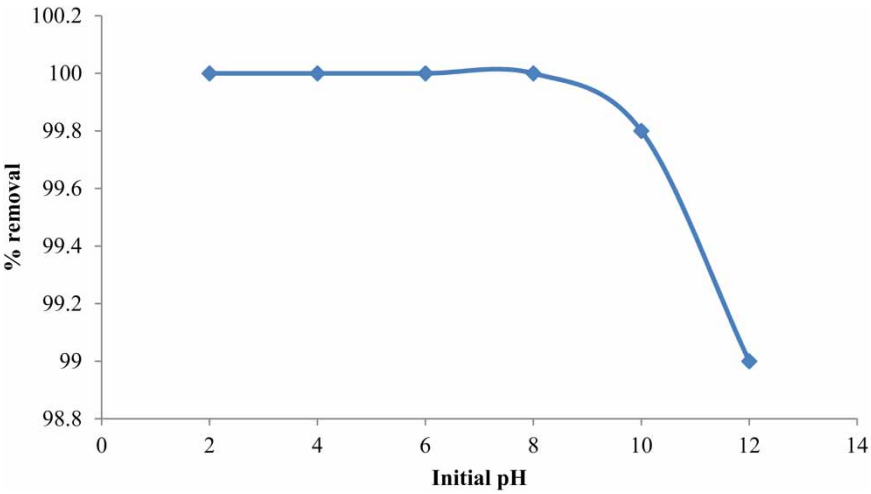

Figure 7 | Percentage removal of fluoride with pH of the solution (conditions: 30 min, 0.5 g, 25 mg L^{-1} of fluoride, 250 rpm shaking speed, and 26 °C room temperature).

the composite may be attributed to a high pH at point of zero charge (pH_{pzc}) of 10. As such at pH <10, the system is removing anions from the aqueous solution as the adsorbent is positively charged attracting anions. On the basis of this, pH of 2–10 was taken to be the optimum pH range for the subsequent experiments.

Modelling of experimental results

Adsorption kinetics

The effect of contact time on removal of fluoride from aqueous solution was evaluated using different kinetic models to reveal the nature of the adsorption process and the rate limiting processes. A Lagergren pseudo-first-order kinetic model is a well-known model that is used to describe mechanisms of adsorption by different adsorbents. It can be written as follows (Shou *et al.* 2015):

$$\ln(q_e - q_t) = \ln q_e - k_1 t \quad (3)$$

where k_1 (min^{-1}) is the pseudo-first-order adsorption rate coefficient and q_e and q_t are the values of the amount adsorbed per unit mass at equilibrium and at time t, respectively. The experimental data were fitted using the pseudo-first-order kinetic model by plotting $\ln(q_e - q_t)$ vs. t, and

the results are shown in Table 1. The pseudo-first-order was applied and it was found to fairly converge with the experimental data. Moreover, the calculated amount of fluoride ions adsorbed by the composite [$q_{e,\ calc}$ (mg g^{-1})] was less than the experimental values [$q_{e,\ exp}$ (mg g^{-1})] (Table 1). The findings indicated that the Lagergren pseudo-first-order kinetic model is inappropriate to describe the adsorption of fluoride ions from aqueous system by the composite.

The pseudo-second-order kinetic model is another kinetic model that is widely used to describe the adsorption process from an aqueous solution. The linearized form of the pseudo-second-order rate equation is given as follows:

$$\frac{t}{q_t} = \frac{1}{k_2 q_e^2} + \frac{t}{q_e} \quad (4)$$

where k_2 [g(mg min^{-1})] is the pseudo-second-order adsorption rate coefficient and q_e and q_t are the values of the amount adsorbed per unit mass at equilibrium and at time t, respectively. An application of the pseudo-second-order rate equation for adsorption of fluoride to the composite matrices portrayed a good fit with the experimental data (Figure 8 and Table 1). The obtained results confirm that the pseudo-second-order model is the most suitable kinetic model to describe adsorption of fluoride ions by the composite from the aqueous system. Moreover, this also confirms that the mechanism of fluoride removal from aqueous solution is chemisorption. To be noted is that the theoretical adsorption capacity is close to the experimental adsorption capacity further confirming that this model describes the adsorption data.

The overall kinetics of the adsorption process may be governed by diffusional processes as well as by the kinetics of the surface chemical reaction. In diffusion studies, the rate is often expressed in terms of the square root of time.

$$q_t = k_{id} t^{1/2} + C_i \quad (5)$$

Table 1 | Different kinetic model parameters for adsorption of fluoride ions on the composite

Adsorption kinetics Parameters	$q_{e,\ exp}$ (mg g^{-1})	$q_{e,\ calc}$ (mg g^{-1})	k_1 (min^{-1})	R^2
Pseudo-first-order	9.9	−357	1.027	0.85
Parameters	$q_{e,\ exp}$ (mg g^{-1})	$q_{e,\ calc}$ (mg g^{-1})	k_2 (g mg^{-1} min^{-1})	R^2
Pseudo-second-order	9.9	10	2.6	1
Parameters	$q_{e,\ exp}$ (mg g^{-1})	C_i (mg g^{-1})	k_{id} (mg g^{-1} $min^{-1/2}$)	R^2
Intra-particle-diffusion	9.9	9.0	0.17	0.7

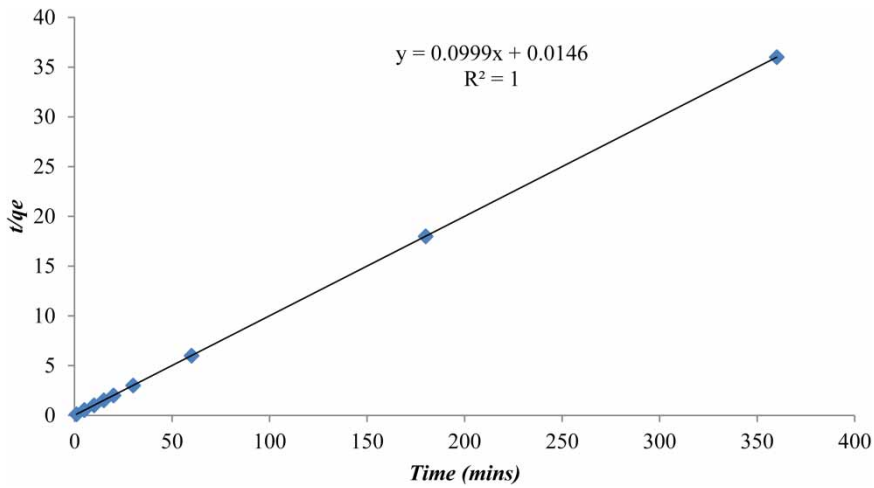

Figure 8 | Pseudo-second-order plot for fluoride adsorption by the composite adsorbent.

where k_{id} (mg g^{-1} min$^{-1/2}$) is the intra-particle diffusion coefficient (slope of the plot of q_t vs. $t^{1/2}$) and C_i is the intra-particle diffusion rate constant. The results show that the intra-particle diffusion model was not applicable for the present process due to the lower correlation coefficients as shown in Table 1. Different kinetic model parameters for the adsorption of fluoride ions onto the composite are shown in Table 1.

Pseudo-second-order plot for fluoride removal by the composite is shown in Figure 8.

Adsorption isotherms

The relationship between the amount of ions adsorbed and the ion concentration remaining in solution can be described by adsorption isotherms. The two most common isotherm types for describing this type of system are Langmuir and Freundlich adsorption isotherms. These models describe adsorption processes on a homogenous (monolayer) or heterogeneous (multilayer) surface, respectively.

The most important model of monolayer adsorption came from Langmuir. This isotherm is given as follows:

$$\frac{C_e}{q_e} = \frac{1}{Q_m b} + \frac{C_e}{Q_m} \tag{6}$$

The essential characteristics of the Langmuir isotherms can be expressed in terms of a dimensionless constant separation factor or equilibrium parameter, R_L, which is defined as:

$$R_L = \frac{1}{1 + bC_o} \tag{7}$$

$R_L > 1$ means unfavourable reaction, $R_L = 1$ means linear fit, $0 < R_L < 1$ means favourable reaction and $R_L = 0$ means irreversible reaction.

Where C_e = equilibrium concentration (mg L^{-1}), Q_e = amount adsorbed at equilibrium (mg g^{-1}), Q_m = Langmuir constants related to adsorption capacity (mg g^{-1}) and b = Langmuir constants related to energy of adsorption (L mg^{-1}). A plot of C_e versus C_e/Q_e should be linear if the data are described by the Langmuir isotherm. The value of Q_m is determined from the slope and the intercept of the plot. It is used to derive the maximum adsorption capacity and b is determined from the original equation and it represents the intensity of adsorption. The Langmuir adsorption isotherm plot is shown in Figure 9.

The Freundlich adsorption isotherm describes the heterogeneous surface energy by multilayer adsorption. The Freundlich isotherm can be formulated as follows:

$$\log q_e = \frac{1}{n}\log C_e + \log K \tag{8}$$

where C_e = equilibrium concentration (mg L^{-1}), q_e = amount adsorbed at equilibrium (mg g^{-1}), K = partition coefficient (mg g^{-1}) and n = intensity of adsorption. The linear plot of log C_e versus log q_e indicates if the data are described

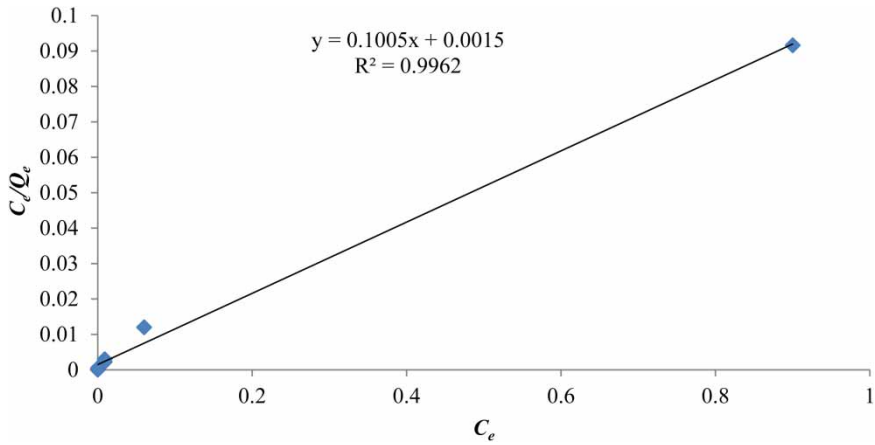

Figure 9 | Langmuir adsorption plot for fluoride adsorption onto the composite adsorbent.

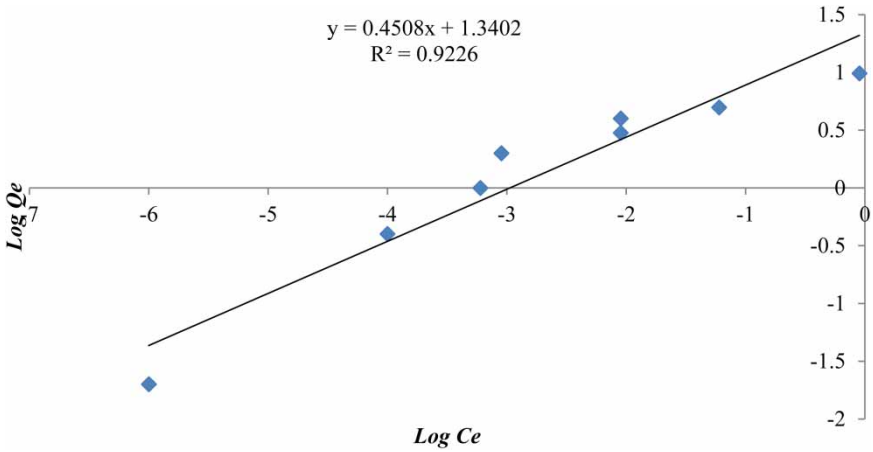

Figure 10 | Freundlich adsorption plot for fluoride adsorption onto the composite adsorbent.

by the Freundlich isotherm. The value of K implies that the energy of adsorption on a homogeneous surface is independent of surface coverage and n is an adsorption constant which reveals the rate at which adsorption is taking place. These two constants are determined from the slope and intercept of the plot of each isotherm. The plot of Freundlich adsorption isotherm is shown in Figure 10.

The parameters of Langmuir and Freundlich adsorption isotherms are shown in Table 2.

As tabulated, the Langmuir isotherm showed a high correlation coefficient ($R^2 > 0.99$) (Figure 9). R_L shows that the reaction of fluoride and the composite was favourable. The Q_m and b show that the adsorption of fluoride by the composite takes place at high energy with high intensity of adsorption. The Freundlich adsorption isotherm also showed a good regression coefficient ($R^2 > 0.90$) (Figure 10). The n value between 0 and 10 shows that the reaction is beneficial and the K_f value shows that it has high adsorption capacity. This indicates a good agreement between the experimental values and isotherm parameters. The data fitted better to the Langmuir adsorption isotherm than the Freundlich adsorption isotherm thus depicting a monolayer adsorption mode.

Table 2 | Langmuir and Freundlich parameters

Adsorption isotherm	Langmuir				Freundlich		
Parameter	R^2	R_L	Q_m	b	R^2	K_f	n
Fluoride	0.99	6×10^{-4}	10	66.7	0.92	21.9	2.2

Removal of fluoride under optimized conditions

Results for the removal of fluoride on raw water under optimized conditions are shown in Table 3. The physiochemical conditions of borehole water before and after defluoridation are also tabulated in Table 4. The fluoride-rich ground water was observed to be slightly alkaline with a pH of 9. The composite was observed to remove fluoride from groundwater to below 0.01 mg L^{-1}. This shows that the composite is an effective material that can be used for the removal of fluoride in groundwater.

Adsorption capacity of the composite as compared to other adsorbents

A comparison of the adsorption capacity of the composite and other adsorbents that have been reported to remove fluoride is shown in Table 4.

Table 4 compares the different adsorption capacities of various adsorbents of fluoride reported in different

Table 3 | Levels of pH, EC, TDS and fluoride before and after treatment

Type of water	Synthetic water		Field water	
Parameter	Raw	Treated	Raw	Treated
pH	8	10	9	10
EC (μS cm^{-1})	145	41.2	100	45.3
TDS (mg L^{-1})	73	27.3	66.4	43
F^- (mg L^{-1})	50	0.01	10	0.01

Table 4 | Comparison of different adsorption capacities (mg g^{-1}) of different adsorbents for fluoride

Adsorbent	Adsorption capacity (mg g^{-1})	References
Magnesite/bentonite composite	10	Present study
Cryptocrystalline magnesite	9.2	Masindi *et al.* (2015b)
Alum-bent	5.7	Masindi *et al.* (2014c)
Al-oxide origin alumina	2	Kamble *et al.* (2010)
Mg^{2+} bentonite	2.3	Thakre *et al.* (2010a)
Polymer/bio-polymer composites	15	Karthikeyan *et al.* (2011)
Activated alumina	1.1	Maliyekkal *et al.* (2006)
La impregnated silica gel	3.8	Zhou *et al.* (2004)
Fe^{3+}modified bentonite clay	2.9	Gitari *et al.* (2013)

literature. Even though the adsorption capacities were obtained at different experimental conditions, they offer a useful criterion to compare the different adsorption capacities. From the table, it is clear that the composite has a higher adsorption capacity as compared to the other adsorbents. Therefore, the composite can be effectively applied for defluoridation of groundwater because of its ability to adsorb fluoride.

CONCLUSIONS

A simple, novel and innovative method for defluoridation was developed to synthesize cryptocrystalline magnesite–bentonite clay composite using a vibratory ball mill. The synthesized composite successfully removed fluoride from aqueous solution. Optimum conditions for the removal of fluoride were 30 min shaking, 0.5 g dosage, 25 mg L^{-1} initial fluoride concentration, pH $\leq$ 10 and 250 rpm shaking speed. Greater than 99% removal efficiency for fluoride was observed at these optimum conditions. The adsorption data fitted better to the Langmuir adsorption isotherm than the Freundlich adsorption isotherm therefore proving monolayer adsorption. Adsorption kinetics fitted better to pseudo-second-order than pseudo-first-order thus indicating chemisorption. This study produced a novel engineered material with better adsorption capacity for fluoride when compared to other conventional methods.

ACKNOWLEDGEMENTS

The authors wish to express their sincere gratitude to the Council of Scientific and Industrial research (CSIR), Environmental Remediation and Water Pollution Chemistry Research Group, University of Venda Directorate, Department of Ecology and Resource Management, ESKOM-TESP, SASOL-Inzalo, and DST-NRF for supporting this project financially.

REFERENCES

Ayoob, S. & Gupta, A. K. 2006 Fluoride in drinking water: a review on the status and stress effects. *Critical Reviews in Environmental Science and Technology* **36**, 433–487.

Bhatnagar, A., Kumar, E. & Sillanpää, M. 2011 Fluoride removal from water by adsorption – a review. *Chemical Engineering Journal* **171**, 811–840.

Bhattacharyya, K. G. & Gupta, S. S. 2008 Adsorption of a few heavy metals on natural and modified kaolinite and montmorillonite: a review. *Advances in Colloid and Interface Science* **140**, 114–131.

Çengeloğlu, Y., Kır, E. & Ersöz, M. 2002 Removal of fluoride from aqueous solution by using red mud. *Separation and Purification Technology* **28**, 81–86.

Dolar, D., Košutić, K. & Vučić, B. 2011 RO/NF treatment of wastewater from fertilizer factory – removal of fluoride and phosphate. *Desalination* **265**, 237–241.

Dukić, A. B., Kumrić, K. R., Vukelić, N. S., Dimitrijević, M. S., Baščarević, Z. D., Kurko, S. V. & Matović, L. L. 2015a Simultaneous removal of Pb^{2+}, Cu^{2+}, Zn^{2+} and Cd^{2+} from highly acidic solutions using mechanochemically synthesized

montmorillonite-kaolinite/TiO_2 composite. *Applied Clay Science* **103**, 20–27.

Đukić, A. B., Kumrić, K. R., Vukelić, N. S., Stojanović, Z. S., Stojmenović, M. D., Milošević, S. S. & Matović, L. L. 2015b Influence of ageing of milled clay and its composite with TiO_2 on the heavy metal adsorption characteristics. *Ceramics International* **41**, 5129–5137.

Emamjomeh, M. M., Sivakumar, M. & Varyani, A. S. 2011 Analysis and the understanding of fluoride removal mechanisms by an electrocoagulation/flotation (ECF) process. *Desalination* **275**, 102–106.

Gitari, W. M., Ngulube, T., Masindi, V. & Gumbo, J. R. 2013 Defluoridation of groundwater using Fe^{3+}-modified bentonite clay: optimization of adsorption conditions. *Desalination and Water Treatment* **53** (6), 1578–1590.

Gong, W.-X., Qu, J.-H., Liu, R.-P. & Lan, H.-C. 2012 Effect of aluminum fluoride complexation on fluoride removal by coagulation. *Colloids and Surfaces A: Physicochemical and Engineering Aspects* **395**, 88–93.

Hou, D., Wang, J., Sun, X., Luan, Z., Zhao, C. & Ren, X. 2010 Boron removal from aqueous solution by direct contact membrane distillation. *Journal of Hazardous Materials* **177**, 613–619.

Jagtap, S., Yenkie, M. K., Labhsetwar, N. & Rayalu, S. 2012 Fluoride in drinking water and defluoridation of water. *Chemical Reviews* **112**, 2454–2466.

Kamble, S. P., Deshpande, G., Barve, P. P., Rayalu, S., Labhsetwar, N. K., Malyshew, A. & Kulkarni, B. D. 2010 Adsorption of fluoride from aqueous solution by alumina of alkoxide nature: batch and continuous operation. *Desalination* **264**, 15–23.

Karthikeyan, M., Kumar, K. K. S. & Elango, K. P. 2011 Batch sorption studies on the removal of fluoride ions from water using eco-friendly conducting polymer/bio-polymer composites. *Desalination* **267**, 49–56.

Kettunen, R. & Keskitalo, P. 2000 Combination of membrane technology and limestone filtration to control drinking water quality. *Desalination* **131**, 271–283.

Khatibikamal, V., Torabian, A., Janpoor, F. & Hoshyaripour, G. 2010 Fluoride removal from industrial wastewater using electrocoagulation and its adsorption kinetics. *Journal of Hazardous Materials* **179**, 276–280.

Kumrić, K. R., Crossed, D., Signukić, A. D. S. B., Trtić-Petrović, T. M., Vukelić, N. S., Stojanović, Z., Grbović Novaković, J. D. & Matović, L. L. 2013 Simultaneous removal of divalent heavy metals from aqueous solutions using raw and mechanochemically treated interstratified montmorillonite/kaolinite clay. *Industrial and Engineering Chemistry Research* **52**, 7930–7939.

Luo, F. & Inoue, K. 2004 The removal of fluoride ion by using metal(III)-loaded amberlite resins. *Solvent Extraction and Ion Exchange* **22**, 305–322.

Maliyekkal, S. M., Sharma, A. K. & Philip, L. 2006 Manganese-oxide-coated alumina: a promising sorbent for defluoridation of water. *Water Research* **40**, 3497–3506.

Maliyekkal, S. M., Anshup, Antony, K. R. & Pradeep, T. 2010 High yield combustion synthesis of nanomagnesia and its application for fluoride removal. *Science of the Total Environment* **408**, 2273–2282.

Masindi, V. & Gitari, W. M. 2016 Simultaneous removal of metal species from acidic aqueous solutions using cryptocrystalline magnesite/bentonite clay composite: an experimental and modelling approach. *Journal of Cleaner Production* **112** (1), 1077–1108.

Masindi, V., Gitari, M. W., Tutu, H. & De Beer, M. 2014a Application of magnesite–bentonite clay composite as an alternative technology for removal of arsenic from industrial effluents. *Toxicological & Environmental Chemistry* **96** (10), 1435–1451.

Masindi, V., Gitari, W. M. & Ngulube, T. 2014c Defluoridation of drinking water using Al^{3+}-modified bentonite clay: optimization of fluoride adsorption conditions. *Toxicological & Environmental Chemistry* **96** (9), 1294–1309.

Masindi, V., Gitari, M. W., Tutu, H. & De Beer, M. 2015a Synthesis of a porous magnesite-bentonite clay composite and its application for neutralisation and attenuation of inorganic contaminants in acidic and metalliferous mine drainage. In: *5th Conference on the Environment ICENV*, Malaysia, Penang, June 2015, pp. 69–77.

Masindi, V., Gitari, W. M. & Ngulube, T. 2015b Kinetics and equilibrium studies for removal of fluoride from underground water using cryptocrystalline magnesite. *Journal of Water Reuse and Desalination* **5** (3), 282–292.

Meenakshi, S. & Viswanathan, N. 2007 Identification of selective ion-exchange resin for fluoride sorption. *Journal of Colloid and Interface Science* **308**, 438–450.

Miretzky, P. & Cirelli, A. F. 2011 Fluoride removal from water by chitosan derivatives and composites: a review. *Journal of Fluorine Chemistry* **132**, 231–240.

Mohapatra, M., Anand, S., Mishra, B. K., Giles, D. E. & Singh, P. 2009 Review of fluoride removal from drinking water. *Journal of Environmental Management* **91**, 67–77.

Onyango, M. S. & Matsuda, H. 2006 Chapter 1. Fluoride removal from water using adsorption technique. In: *Advances in Fluorine Science* (T. Alain, ed.). Elsevier, Amsterdam, pp. 1–48.

Ruixia, L., Jinlong, G. & Hongxiao, T. 2002 Adsorption of fluoride, phosphate, and arsenate ions on a new type of ion exchange fiber. *Journal of Colloid and Interface Science* **248**, 268–274.

Sandoval, M. A., Fuentes, R., Nava, J. L. & Rodríguez, I. 2014 Fluoride removal from drinking water by electrocoagulation in a continuous filter press reactor coupled to a flocculator and clarifier. *Separation and Purification Technology* **134**, 163–170.

Shen, J. & Schäfer, A. 2014 Removal of fluoride and uranium by nanofiltration and reverse osmosis: a review. *Chemosphere* **117**, 679–691.

Shou, J., Jiang, C., Wang, F., Qiu, M. & Xu, Q. 2015 Fabrication of Fe_3O_4/MgAl-layered double hydroxide magnetic composites for the effective decontamination of Co(II) from synthetic wastewater. *Journal of Molecular Liquids* **207**, 216–223.

Srimurali, M., Pragathi, A. & Karthikeyan, J. 1998 A study on removal of fluorides from drinking water by adsorption onto low-cost materials. *Environmental Pollution* **99**, 285–289.

Thakre, D., Jagtap, S., Sakhare, N., Labhsetwar, N., Meshram, S. & Rayalu, S. 2010a Chitosan based mesoporous Ti–Al binary metal oxide supported beads for defluoridation of water. *Chemical Engineering Journal* **158**, 315–324.

Thakre, D., Rayalu, S., Kawade, R., Meshram, S., Subrt, J. & Labhsetwar, N. 2010b Magnesium incorporated bentonite clay for defluoridation of drinking water. *Journal of Hazardous Materials* **180**, 122–130.

Tor, A. 2006 Removal of fluoride from an aqueous solution by using montmorillonite. *Desalination* **201**, 267–276.

Trikha, R. & Sharma, B. K. 2014 Studies on factors affecting fluoride removal from water using passive system. *Journal of Environmental Chemical Engineering* **2**, 172–176.

Turner, B. D., Binning, P. & Stipp, S. L. S. 2005 Fluoride removal by calcite: evidence for fluorite precipitation and surface adsorption. *Environmental Science and Technology* **39**, 9561–9568.

Vasudevan, S., Lakshmi, J. & Sozhan, G. 2011 Studies on the Al–Zn–In-alloy as anode material for the removal of chromium from drinking water in electrocoagulation process. *Desalination* **275**, 260–268.

Viswanathan, N. & Meenakshi, S. 2010 Enriched fluoride sorption using alumina/chitosan composite. *Journal of Hazardous Materials* **178**, 226–232.

Wang, P., Wang, Z., Wu, Z., Zhou, Q. & Yang, D. 2010 Effect of hypochlorite cleaning on the physiochemical characteristics of polyvinylidene fluoride membranes. *Chemical Engineering Journal* **162**, 1050–1056.

Yu, Y., Yu, L. & Paul Chen, J. 2015 Adsorption of fluoride by Fe–Mg–La triple-metal composite: adsorbent preparation, illustration of performance and study of mechanisms. *Chemical Engineering Journal* **262**, 839–846.

Zhang, C., Chen, L., Wang, T.-J., Su, C.-L. & Jin, Y. 2014 Synthesis and properties of a magnetic core–shell composite nano-adsorbent for fluoride removal from drinking water. *Applied Surface Science* **317**, 552–559.

Zhou, Y., Yu, C. & Shan, Y. 2004 Adsorption of fluoride from aqueous solution on La^{3+}-impregnated cross-linked gelatin. *Separation and Purification Technology* **36**, 89–94.

Zhu, P., Wang, H., Sun, B., Deng, P., Hou, S. & Yu, Y. 2009 Adsorption of fluoride from aqueous solution by magnesia-amended silicon dioxide granules. *Journal of Chemical Technology and Biotechnology* **84**, 1449–1455.

Zulfiqar, M., Omar, A. A. & Chowdhury, S. 2014 Removal of phosphate and fluoride from industrial wastewater – a short review. *Applied Mechanics and Materials* **625**, 805–808.

First received 14 March 2016; accepted in revised form 27 May 2016. Available online 7 July 2016